Chapter 4

Magnetic properties of the layer systems measured by SQUID magnetometry

4.1 Introduction

There is a variety of phenomena related to the different exchange bias systems. One of the most obvious features in EB systems, described in chapter 2, is the dependence of the EB field upon the FM layer thickness. The strength of the EB field was found to decrease with increasing FM layer thickness $\sim \frac{1}{d_{FM}}$. Therefore it could be concluded that the EB is exclusively an interface effect. However, recently it was experimentally shown that magnetic coupling might also occur across a non-magnetic spacer in FM/spacer/AFM systems [GAC97] [Mew00] [TKP00]. The EB effect was then suggested to be long-range and possibly to have parallel analogies to FM/spacer/FM systems [GSP$^+$86], [PMR90].

The phenomenon of long-range oscillatory exchange coupling between ferromagnetic films across non-magnetic spacers was discovered about 10 years ago [PMR90]. Successive ferromagnetic layers have been found to couple variously in either AFM or FM arrangements depending on the thickness and specific electronic structure of the spacer material. This effect is of great technological importance since it allows the design of specific systems, such as e.g. artificial EB systems, just by varying the spacer thickness. Oscillatory exchange coupling has been established as a general phenomenon relevant for many spacer materials such as the non-magnetic d-transition metals and the noble metals.

In contrast to FM/spacer/FM systems only few systems of the type FM/-spacer/AFM have been studied so far. The experimental findings in that new

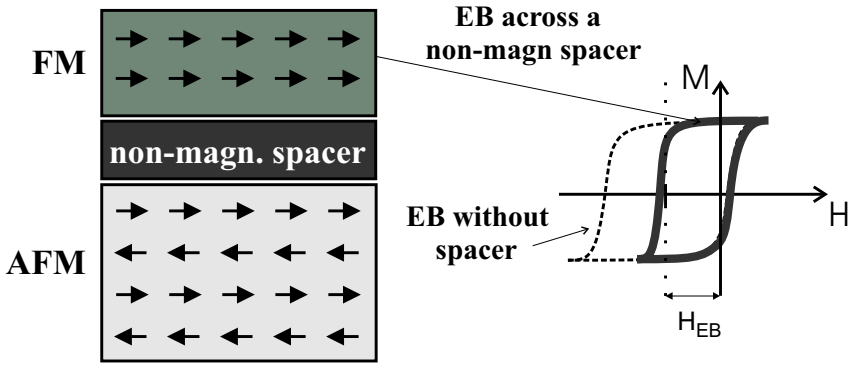

Figure 4.1: EB across a non-magnetic spacer.

area of interest led to some controversy as to whether the EB across non-magnetic spacers is long-range [GAC97, Mew00] or has to be attributed to the existence of pinholes [TKP00].

In all cases where the EB strength has been investigated as a function of the spacer thickness, the EB field H_{EB} was found to decrease with increasing spacer thickness. It vanishes above a critical spacer thickness, which has proved to be material dependent [GAC97, Mew00, TKP00]. Together with H_{EB} also the coercive field is reduced (illustrated schematically in Fig. 4.1) as the spacer thickness is increased.

For some systems, e.g. $Ni_{81}Fe_{90}$/(Cu,Ag,Au)(x)//CoO(111) [GAC97], the strength of the EB shift has been found to decrease exponentially with increasing spacer thickness and was suggested to be long-ranged. The decrease was characterized by a decay length L which depends on the spacer material.

In other studies on $Co_{84}Fe_{16}$/spacer/$Ir_{22}Mn_{78}$ trilayers, with different spacers, such as Al, Ag, Au, Si, Pd, Ru and Ti [TKP00], only very small decay length have been found. In that case the overall behavior has been attributed to the existence of pinholes in the spacer material.

In any case, it has not been established yet whether interlayer exchange coupling in FM/spacer/AFM systems is a general phenomenon.

In this chapter, SQUID magnetometry measurements will be presented where the EB coupling strength in Co/Au/CoO trilayers has been investigated as a function of the spacer thickness to further elucidate the character of the coupling between FM and AFM across a spacer. The corresponding Co/CoO bilayer system is characterized by extraordinarily high exchange bias shifts (45 mT) providing a high sensitivity, even for spacers in the critical spacer thickness range. Therefore it is well suited for the investigations of possible long range coupling. Furthermore the present Co/CoO bilayers with only 2 nm

thin CoO are characterized by hysteresis loops of rectangular shape and by an ideal dependence upon the Co layer thickness.

In addition, the magnetic properties of a $[Co/CoO/Au]_{20}$ multilayer, deposited on $Al_2O_3(0001)$, have been investigated via SQUID magnetometry. The results will be presented in this chapter. Except for the choice of the substrate, the multilayer was prepared under similar conditions as the bi-/trilayer systems. The aim of this investigation is to demonstrate that the characteristic features of the simple bilayer are maintained in the multilayer structure, where the 3.4 nm thick Au layers serve to separate the individual Co/CoO bilayers from each other. From the previously-described investigations on Co/Au/CoO trilayers this Au layer thickness was proved to be above the critical thickness where possible coupling across the spacer might occur. The multilayer will be used for investigations via polarized neutron reflectometry. For this type of measurements a multilayer is better suited, since it provides a much higher signal to noise ratio than the corresponding bilayer system.

In the next section the experimental method and setup of a SQUID magnetometer will be briefly described. The experiments and the results are presented in the section thereafter, followed in the last section by the conclusions.

4.2 SQUID magnetometry

A SQUID (**S**uperconducting **Q**uantum **I**nterference **D**evice) magnetometer of the type Quantum Design MPMS2 (**M**agnetic **P**roperties **M**easurement **S**ystem) was used to study the macroscopic magnetic properties of the EB samples. The MPMS device is basically a ^{4}He cryostat with a superconducting magnet wherein the sample temperature can be controlled by a ^{4}He gas flow control system. The core of the apparatus is the SQUID detector, and the measured quantity is the electronic magnetic dipole moment m_z of a sample with respect to the direction parallel to the applied magnetic field. A scheme of the technical setup of the SQUID magnetometer is given in Fig. 4.2.

To investigate the magnetic properties of a sample, it is exposed to the homogenous field of a superconducting magnet and gradually moved through the pick-up coil system, which is essentially an arrangement of induction coils. The coils are wound in a configuration in which the upper and lower single turns are counterwound with respect to the two-turn center coil. This configuration strongly rejects interference from nearby magnetic sources and allows the system to function without the need for a superconducting shield around the SQUID sensing loop. While passing the coil arrangement stepwise, a magne-

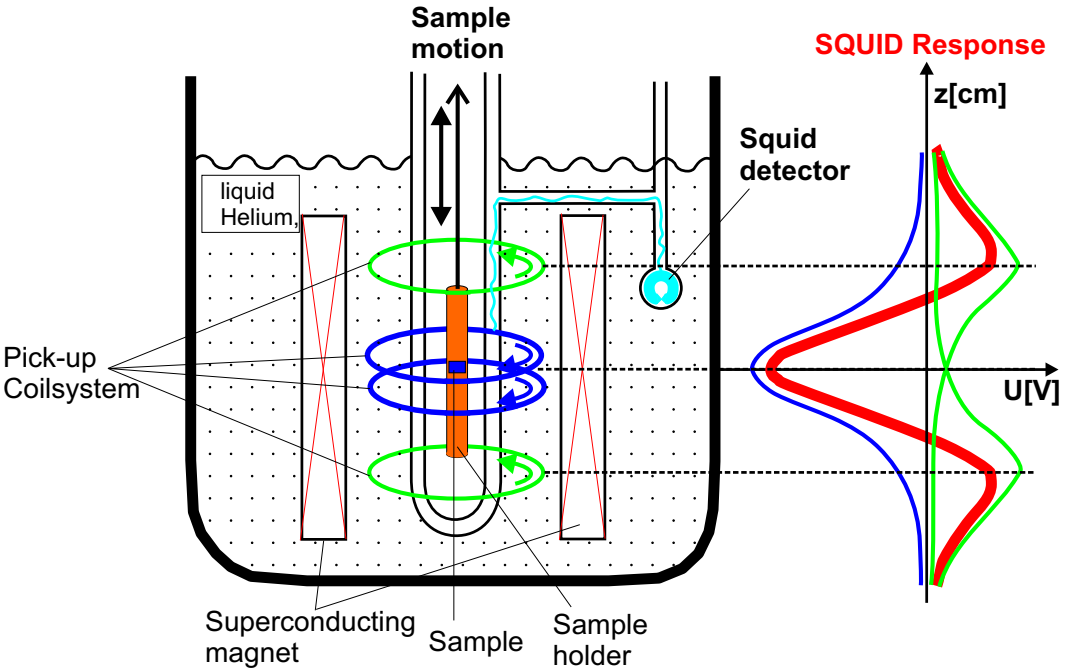

Figure 4.2: Scheme of the SQUID setup.

tized sample induces a voltage at each step. The SQUID detector itself, which is a Josephson contact loop, serves to precisely measure the induced voltage. The sensor is a superconducting ring which is at one or at several positions quasi-interrupted (e.g. a by point contact), yielding so called weak-links. At these positions the critical current is significantly reduced. With the help of a sophisticated technique it is achieved that the magnetic flux inside the ring does not change with time: therefore each additional flux quantum has to be compensated with a dc current. The magnitude of this current, which is proportional to the number of magnetic flux quanta, is a measure of the change of the magnetic flux density caused by the magnetization of the sample as it is moved through the pick-up coil system. If the SQUID voltage is read at a large number of points, the voltage can be plotted as a function of the sample position. A set of such data is a scan and typically called the SQUID response. As illustrated in Fig. 4.2 the shape of the curve is a function of the detection coil geometry used in the MPMS system. The SQUID response is fitted using the MPMS2 software to yield the sample magnetization. Usually a sample is cycled several times through the pick-up coil system at a constant field and at constant temperature. The single results are then summed and averaged.

4.3 Results and discussion

4.3.1 Investigations of Co/Au/CoO trilayer systems

For the investigation of the EB effect across a non-magnetic spacer between FM and AFM layers, various Co(16.4 nm)/Au(x)/CoO(2 nm) trilayers with different Au spacer thicknesses d_{Au} between 0.25 nm and 6 nm were measured by SQUID magnetometry. The trilayers are protected against contamination in air by a 4 nm Au capping layer. After field cooling the sample in a field of +400 mT, hysteresis measurements were performed at 10 K as a function of the spacer thickness d_{Au}. The measurements were started at an external field of +150 mT, where the FM Co was saturated, and the starting field was parallel to the cooling field direction. The results are plotted in Fig. 4.3a,b. In a) the hysteresis loops for samples with Au spacer thicknesses between 0.25 nm and 1.5 nm are presented, whereas in b) the results with thicker Au spacers between 1.75 nm and 2.25 nm are presented. It is obvious that the hysteresis loops from samples containing thinner Au spacers are characterized by an almost ideal rectangular shape at the first magnetization reversal, i.e. at the coercivity H_{CA} (**C**oercivity **A**ntiparallel to the cooling field direction) for decreasing fields. The magnetization remains close to saturation before a sudden reversal to the negative saturated state takes place. For the samples with thicker Au spacers, the magnetization slightly decreases before the magnetization is completely reversed to the opposite direction. In the case of the second magnetization reversal, i.e. at the coercivity H_{CP} (**C**oercivity **P**arallel to the cooling field direction) for increasing fields, the shape of the hysteresis loop is rounded for all samples. This rounding is even stronger for the samples containing thicker Au spacers. The observed asymmetry on opposite sides of the hysteresis loop indicates asymmetric magnetization reversal processes and will be treated further in the following paragraph.

For clarity in Fig. 4.4 the coercive fields $|H_{CA}|$ and H_{CP}, as defined above, and $H_C = \frac{1}{2}(|H_{CA}| + H_{Cp})$, are plotted as a function of the Au spacer thickness. It is clearly visible from the plot that $|H_{CA}|$ continuously decreases with increasing Au spacer thickness, while H_{CP} is characterized by an almost constant negative value between -9 mT and -7 mT for the samples with thinner Au spacers.

As the Au spacer thickness was increased above 1.75 nm, H_{CP} dropped to a value close to zero field (Fig. 4.3), which means that the whole hysteresis loops shift closer to zero field. Additionally the remanent magnetization decreases to 90% of the saturation value.

Normalizing the exchange bias field $H_E = \frac{1}{2}|H_{CA}+H_{CP}|$ with $H_{E0} = 45$ mT [GR00a], the field obtained for a simple Co(16.4 nm)/CoO(2 nm) bilayer with-

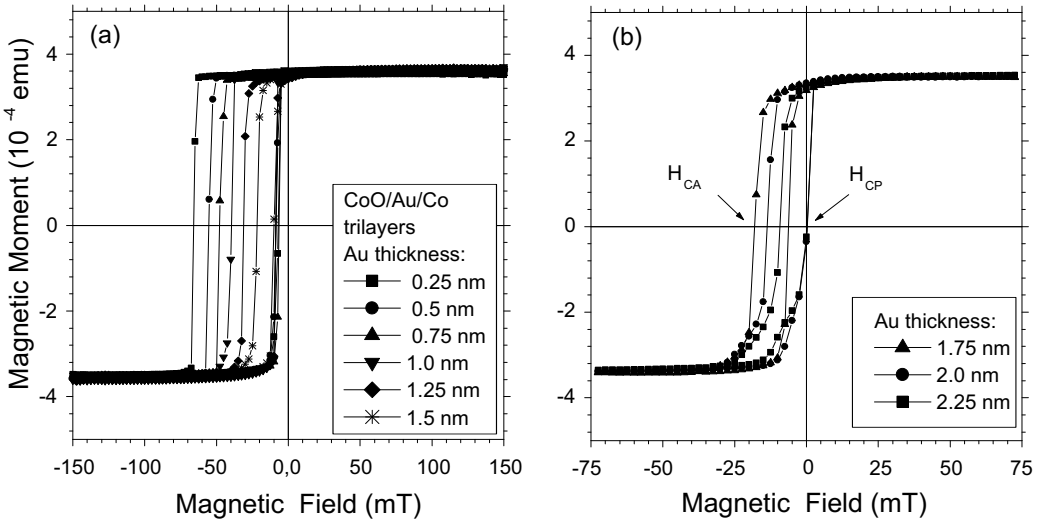

Figure 4.3: Magnetic hysteresis loops at T = 10 K for 2 nm CoO/x nm Au/16.4 nm Co trilayers with different Au spacer thicknesses performed after cooling in a field H_{cool}=+400 mT from T=320 K. (a) x=0.25; 0.5; 0.75; 1.0; 1.25 and 1.5 nm and (b) x=1.75; 2.0; and 2.25 nm.

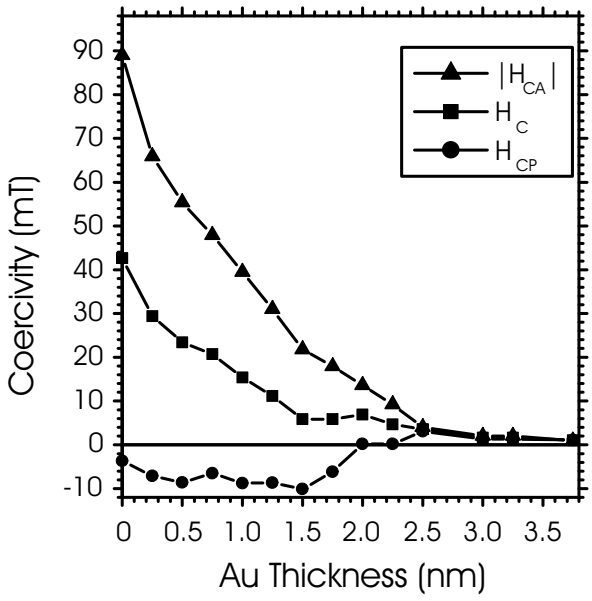

Figure 4.4: Coercivities $|H_{CA}|$, H_{CP} and H_C at $T = 10\ K$ as a function of the Au spacer thicknesses in 2 nm CoO/x nm Au/16.4 nm Co trilayers.

out spacer, and plotting it as a function of the Au spacer thickness, leads to Fig. 4.5. The right axis of this figure indicates a lower limit for the interfacial coupling energy $E^*_{int} = H_E \cdot M_S \cdot d_{Co}$, which is defined as the product of the exchange bias field H_E, the magnetization M_S and the thickness d_{Co} of the FM Co layer. AT 10 K this energy amounts to 1.03 $\frac{erg}{cm^2}$ for the simple Co/CoO bilayer, which is one of the highest values ever obtained for EB systems [JS99]. Fig. 4.5 further reveals that the strength of the EB field decreases monotonically with increasing Au spacer thickness up to the critical thickness of 2.5 nm, where the EB almost vanishes, while at 2.25 nm H_{EB} still amounts 4.5 mT, corresponding to a coupling strength of 0.1 erg/cm^2. It should be noted that for the majority of the EB systems investigated, a value of 4.5 mT is obtained only in the full coupling limit, i.e. without a spacer [JS99].

Certainly the present data do not show any indication of an oscillatory behavior of the EB coupling strength superimposed onto the monotonic decrease, as was found by Mewes *et al.* [Mew00]. The strength of the oscillatory contribution, as observed by Mewes *et al.* was found to be about an order of magnitude smaller than the monotonic decrease onto which it was superimposed. The observation of oscillatory coupling requires some coherency of propagating spin dependent electron waves, which would be destroyed by roughness. It cannot be excluded that the absence of oscillatory coupling in the present Co/Au/CoO systems could be due to interfacial roughness.

In order to describe the dependence of the EB coupling strength upon the spacer thickness it was suggested by Gökemeijer *et al.* [GAC97] to use an exponential fit of the form $H_E = H_{E0}\ exp(-\frac{d_{Au}}{L})/d^n_{Au}$, with the characteristic decay length L and an integer n.

An exponential decrease with n = 2 has been used to describe the interlayer exchange coupling in FM/spacer/FM systems. In the experiments on $Ni_{81}Fe_{19}(30\ nm)/noble\ metal(x)/CoO(30\ nm)$ EB-multilayers (Fm/spacer/-AFM type), performed by Gökemeijer *et al.* [GAC97], the dependence of the exchange coupling upon the spacer thickness could be fitted successfully by a simple exponential expression taking the exponential $n = 0$. For the noble metals Au and Ag, relatively high values for the decay length L have been reported: L_{Ag}=1.73 nm and L_{Au}=0.92 nm, while the decay length for copper as spacer material in the above-mentioned multilayer, L_{Cu}=0.41 nm, is considerably reduced. Experiments on $Ni_{81}Fe_{19}(5\ nm)/Cu(x)/FeMn(10\ nm)$ systems, performed by Mewes *et al.* [Mew00], led to even smaller decay lengths of L_{Cu}=0.3 nm.

Attempting to fit the present data, a simple exponential decay fit (i.e. $n = 0$) was added to the experimental data plotted in Fig. 4.5 (solid line). It is obvious that this fit does not reproduce the dependence of the EB strength upon the spacer thickness in Co/Au/CoO trilayers. Only the initial decrease

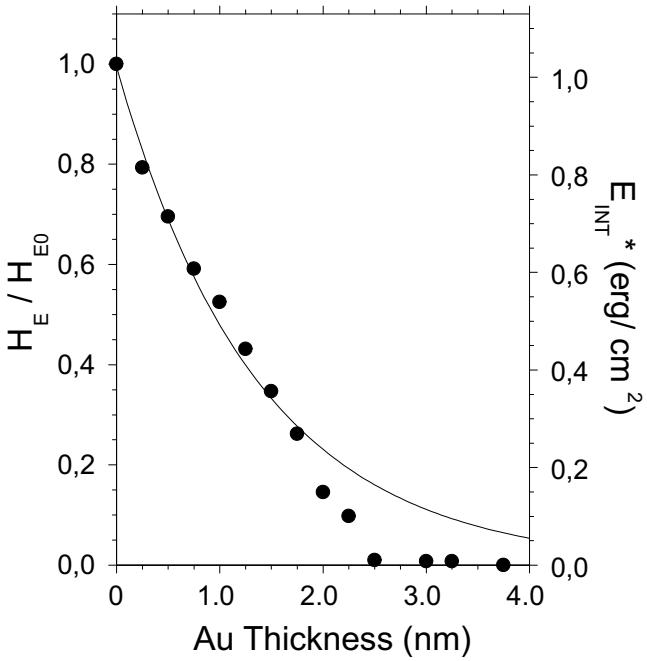

Figure 4.5: The dependence of the normalized exchange bias field $\frac{H_E}{H_{E0}}$ and the coupling strength E^*_{int}=H_E· M_S· d_{Co} on Au spacer thickness d_{Au} (at $T = 10$ K), where H_{E0} is the exchange bias field of the CoO/Co bilayer system. Following Gökemeijer, [GAC97]), an exponential fit (solid line) was added to the data, but it obviously cannot describe the observed behavior.

for small Au spacers up to d_{Au}=1.75 nm follows the exponential fit, whereas above this thickness, the experimental data decrease more rapidly than the fit.

The value of the decay length L may be used as a measure of the range of the interfacial coupling. From the fit a value L_{Au}=1.35 nm can be calculated using the formula given above for an exponential fit with $n = 0$. However, to describe the overall behavior of the EB coupling strength for the present system as a function of an increasing Au spacer thickness, a linear fit would be the most suitable.

For thin Au spacers the interfacial coupling strength, characterized by E^*_{int} and H_E, is already strongly reduced with respect to the values obtained for the simple Co/CoO bilayer. For the trilayer systems containing 0.25 nm and 0.5 nm thick Au spacers this reduction amounts to 20% and 30%, respectively, although for such small spacers the films are likely not to be continuous. Discontinuities imply varying coupling strength along the interface leading to steps or a strong curvature in the hysteresis loops which is not observed for

the present curves. The simple shape of the hysteresis curves, which is maintained up to spacer thicknesses of 1 nm, may be interpreted as due to a reversal of the whole FM Co layer initiated in regions where the interfacial exchange fields are considerably reduced. This local reduction of the exchange coupling strength, caused by the Au spacer, may also modify the effectiveness of AFM domain walls as pinning centers for propagating domain walls in the FM material [LNkS00]. Thus for thinner Au spacers the presence of pinholes is very likely, but the strong decrease of the coupling strength for very small spacer thicknesses indicates that the number of pinholes is rapidly reduced as the spacer thickness is increased. Furthermore the structural analysis, as given in chapter 3, strongly indicates that the thicker Au films are continuous and therefore it can be assumed that the FM and AFM layers are completely separated.

4.3.2 Investigations of a $[Co/CoO/Au]_{20}$ multilayer

A [Co(16.4 nm)/CoO(2 nm)/Au(3.4 nm)]$_{20}$ multilayer was likewise examined by SQUID magnetometry. The preparation and structural features of the multilayer are addressed in chapter 3. The hysteresis loop of the $[Co/CoO/Au]_{20}$ multilayer, grown on $Al_2O_3(0001)$, is characterized by a rectangular shape, as can be seen from Fig. 4.6. Its shape is similar to that of the corresponding bilayer (not plotted here), which was also grown on Al_2O_3. Both systems reveal an extraordinarily high EB of about 40 mT at 10 K.

In comparison to the bilayers grown on H-Si(111), the EB strength of comparable bilayers grown on sapphire is slightly reduced.

In addition, the second magnetization reversal at increasing fields, i.e. at the coercivity H_{CP}, occurs at small positive fields. For the sample grown on H-Si(111), this reversal occurs at small negative fields, indicating that the strength of the AFM is slightly different for the two systems. The latter can possibly be attributed to slightly different interfacial properties for the two samples, such as different grain sizes of the Co and CoO layers (see STM images in chapter 3). The grains are smaller for the bilayer grown on H-Si(111), which therefore has more grain boundaries and thus a larger number of possible pinning centers for domain walls.

But the overall behavior does not change significantly when using an Al_2O_3 substrate, as can be seen from the SQUID measurements.

The high interfacial coupling energy for the present systems can be attributed to a net magnetization at the AFM interface arising from a large number of uncompensated spins. This has been experimentally shown by Gruyters *et al.* [GR00a]. Performing SQUID measurements on granular Co/CoO bilayers on H-Si(111) substrates, prepared in a similar manner as those described

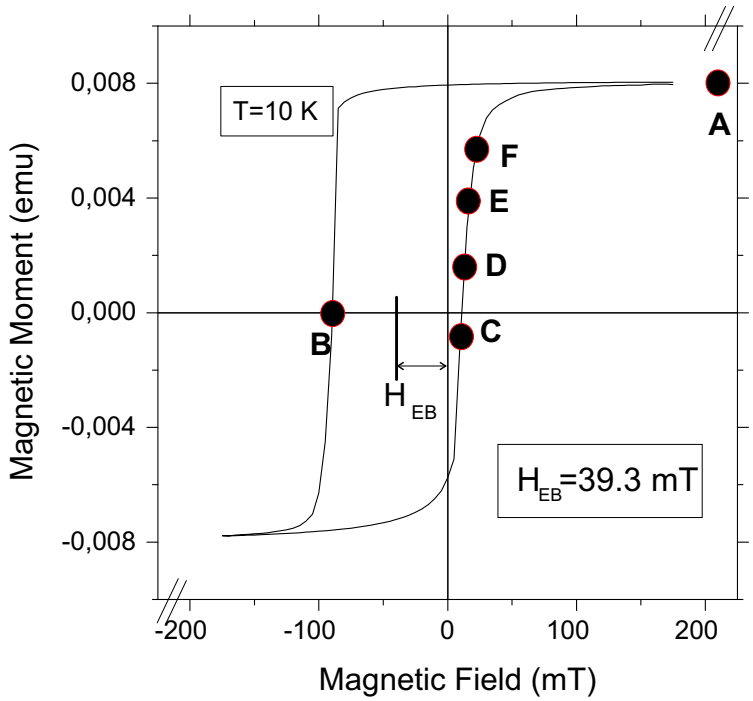

Figure 4.6: Hysteresis of the [Co(16.4 nm)/ CoO(2.0 nm)/ Au(3.4 nm)]$_{20}$ exchange-bias multilayer measured at 10 K after field cooling in a field of 400 mT. The dots mark the positions in the magnetization reversal process where PNR spectra were taken.

above, Gruyters *et al.* observed an extremely strong exchange bias. The high coupling energy in this particular system was found to originate from a single dense layer of independent AFM grains in connection with a large number of uncompensated spins.

A net magnetization in polycrystalline CoO/MgO multilayers has been measured also by Takano *et al.*; it presumably was caused by uncompensated spins at the interfaces [TKB$^+$97]. They found the temperature dependence of the net magnetization to be the same as the temperature dependence of the exchange anisotropy in a multilayer in which similar CoO films are grown next to $Ni_{80}Fe_{20}$ films. This finding demonstrates the importance of uncompensated interfacial AFM spins for the EB coupling mechanism.

The dependence of the EB shift upon defects in the AFM material as possible pinning centers for domain walls has been experimentally confirmed also by Miltényi *et al.* [MGK$^+$00].

Additionally, a closer look on the hysteresis loop of both the multilayer and

the bilayers, grown on different substrates, reveals asymmetric magnetization reversal processes on opposite sites of the same curve. Asymmetric magnetization reversal processes have been found for several EB systems and they have also been addressed theoretically [MSBK87], [SM99a], [Nik98].

The present observed behavior resembles a simple one-dimensional model for EB based on domain wall formation in the AFM [MSBK87]. The sudden reversal at H_{CA} may be interpreted by an irreversible jump of the magnetization in one direction (i.e. opposite to the cooling field direction), while the rounded shape at H_{CP} is attributed to a small region of reversible rotation. However this model does not account for the large coercivities which are also observed in the present system.

A more sophisticated model for EB in polycrystalline FM/AFM films, proposed by Stiles *et al.* [SM99a, SM99b, SM01], accounts for many of the observed effects occurring in the present systems: the unidirectional anisotropy, enhanced coercivities [SM01] and asymmetric magnetization reversal processes [SM99b]. According to this model, independent AFM grains are coupled to a FM film by direct coupling to the interfacial net moments of the grains. Reversing the magnetization in the sample applies a torque to the AFM spins at the interface of each grain which then winds up partial domain walls in the AFM. The model explains the unidirectional anisotropy leading to shifted hysteresis loops, as caused by grains where the AFM ordering is stable as the magnetization is reversed. Energy losses in the antiferromagnet due to irreversible transitions of the AFM ordering in the grains upon magnetization reversal is a possible mechanism causing enhanced coercivities. This latter model appears to be well suited to explain the behavior of the present systems containing granular FM and AFM films.

In Fig.4.7 the temperature dependencies of the H_{EB} field as well as that of the coercive fields present in a simple Co/CoO bilayer (left) and in a $[Co/CoO/Au]_{20}$ multilayer (right), both grown on Al_2O_3, are plotted as a function of the temperature. It has to be noted that the absolute values of the EB field are larger for the bilayer than for the multilayer at a given temperature, since the FM layer in the bilayer system is thinner (14.8 nm) compared to the individual FM layers in the multilayer system (16.4 nm). The plots reveal that the characteristic features of the simple Co/CoO bilayer are maintained in the multilayer. The blocking temperature T_B of about 200 K for both systems is higher than that obtained for a similar bilayer grown on H-Si(111) (175 K) [GGR01], but it is still far below the Néel temperature T_N of CoO. An almost identical temperature behavior of the exchange bias field and very similar magnetic hysteresis loops for the Co/CoO bilayers and the multilayer imply the same AFM/FM coupling mechanism for both types of systems. The increased blocking temperature T_B can be explained by the slightly increased

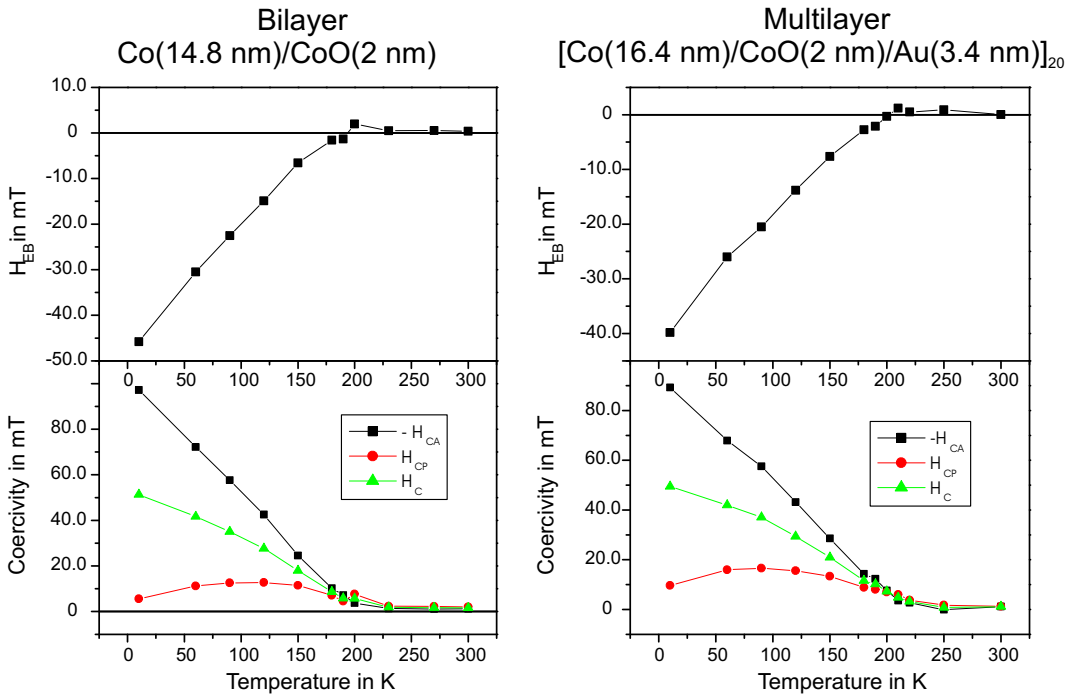

Figure 4.7: Temperature dependence of the exchange bias shift H_{EB} and of the coercive field $H_C = \frac{|H_{CA}|+H_{CP}}{2}$. Left: Co(14.8 nm)/CoO(2 nm)bilayer. Right: $[\text{Co(16.4 nm)/CoO(2 nm)/Au(3.4 nm)}]_{20}$ multilayer.

CoO particle size in the case of Al_2O_3. The linear dependence of H_{EB} on the temperature is in good agreement with reports on other Co/CoO bilayers [GGR01] [MGK+00] [RES+02]. The previously mentioned model by Stiles *et al.* accounts for the observed low blocking temperatures [SM99a]. The experimental finding of $T_B \sim \frac{2}{3}T_N$ is quantitatively explained by thermal instabilities of the AFM state in grains smaller than a certain size [SM99a].

4.4 Conclusion and summary of the SQUID results

In summary, the EB effect across a non-magnetic Au spacer in Co/spacer/CoO trilayers has been investigated as a function of the spacer thickness. It was found that the strength of EB is rapidly suppressed with increasing spacer thicknesses until it vanishes for a 2.5 nm thick Au film. In order to detect possible long-range coupling for Au thicknesses in the critical thickness range,

the Co/CoO system chosen provides very high coupling strengths in the full coupling limit, i.e. without a spacer. In fact, even for a 2.25 nm thick Au film, a coupling strength of 0.1 erg/cm^2 was found. At this thickness a detailed structural analysis confirming that the FM and AFM layer are well separated leads to the conclusion that EB originates not necessarily from nearest-neighbor (direct exchange) or next-nearest-neighbor (superexchange) interactions. As opposed to investigations on other layer systems, as given in Ref. [GAC97] and [Mew00], the present data do not confirm an exponentially decreasing dependence of the EB coupling strength upon the spacer thickness, but show an almost linear decrease. From a comparison of the present results with those obtained by other groups, the dominant process for the EB coupling across a non-magnetic spacer, in particular for small spacer thicknesses, is certainly coupling through pinholes. Beyond this, there is strong experimental evidence that EB coupling occurs even across thicker continuous spacer films. However, from the present data it is assumed that sufficiently strong coupling is limited to about 2.5 nm from the interface.

The present investigations of a $[Co/Co/Au]_{20}$ multilayer provide complementary results and will be compared to the PNR measurements, which are the subject of the next chapter. The SQUID measurements revealed that the characteristic EB features of a simple comparable Co/CoO bilayer are conserved in the multilayer structure. Therefore it can be concluded that the individual bilayers are well separated by the 3.4 nm thick Au spacers. From the previously described results on Co/Au/CoO trilayers this was expected, since any possible interlayer coupling was found to vanish for spacer thicknesses above 2.5 nm. In comparison to the bilayers grown on H-Si(111), only minor differences of the overall behavior as a function of the magnetic field and of the temperature were noticed. They are attributed mainly to the different grain size in the Co and CoO layers in the systems grown on different substrates.